Available online at www.sciencedirect.com
SCIENCE DIRECT®
PERGAMON
International Journal of Multiphase Flow 29 (2003) 291–304
International Journal of Multiphase Flow
www.elsevier.com/locate/ijmulflow

Interfacial area transport of bubbly flow under microgravity environment ☆

T. Takamasa [a,*], T. Iguchi [a], T. Hazuku [a], T. Hibiki [b], M. Ishii [c]

[a] *Faculty of Marine Science, Tokyo University of Mercantile Marine, Etchujima, Koto, Tokyo 135-8533, Japan*
[b] *Research Reactor Institute, Kyoto University, Kumatori, Sennan, Osaka 590-0494, Japan*
[c] *School of Nuclear Engineering, Purdue University, 400 Central Drive West Lafayette, IN 47907-2017, USA*

Received 1 July 2001; received in revised form 10 October 2002

Abstract

In relation to the development of the interfacial area transport equation, axial developments of one-dimensional void fraction, bubble number density, interfacial area concentration, and Sauter mean diameter of adiabatic nitrogen–water bubbly flows in a 9 mm-diameter pipe were measured by using an image-processing method under microgravity environment. The flow measurements were performed at four axial locations (axial distance from the inlet normalized by the pipe diameter = 7, 30, 45 and 60) under various flow conditions of superficial gas velocity (0.0083–0.022 m/s) and superficial liquid velocity (0.073–0.22 m/s). The interfacial area transport mechanism under microgravity environment was discussed in detail based on the obtained data and the visual observation. These data can be used for the development of reliable constitutive relations which reflect the true transfer mechanisms in two-phase flow under microgravity environment.

Keywords: Multiphase flow; Two-fluid model; Interfacial area transport; Bubbly flow; Microgravity environment; Bubble coalescence; Bubble breakup; Wake entrainment

☆ This paper was presented in the 4th International Conference on Multiphase Flow (ICMF-2001). The ICMF-2001 took place in New Orleans, USA during the week of May 27 to June 1, 2001 and was attended by 630 delegates representing 46 countries. Professor E.E. Michaelides was the chair of the conference.

* Corresponding author. Tel: +81-3-5245-7406; fax: +81-3-5245-7410.
E-mail addresses: takamasa@ipc.tosho-u.ac.jp (T. Takamasa), hibiki@rri.kyoto-u.ac.jp (T. Hibiki), ishii@ecn.purdue.edu (M. Ishii).

0301-9322/03/$ - see front matter
PII: S0301-9322(02)00129-5

1. Introduction

For a spacecraft, the major thermal problem is currently to remove the heat generated by crew and other devices from the inside of the spacecraft into the space, in order to ensure acceptable internal environmental conditions. To date, spacecraft active thermal control has been accomplished by using pumped single-phase liquid loops (Di Marco, 1997), which is termed active thermal control systems (ATCSs). The ATCSs have been adopted in the thermal-hydraulic design of the spacecrafts such as Mercury, Gemini and Apollo, and are currently used in the US Space Shuttle, Russian Soyuz spacecraft and MIR space station. However, for larger spacecrafts like the International Space Station, the application of thermal bus or two-phase thermal control system is being developed to accomplish the design of high efficiency heat removal system, which allows of (1) removing relatively high local heat load on the order of tens of kilowatts, (2) conveying the heat for a long distance easily, and (3) controlling the heat load and sink temperature in each modules easily (Grigoriev et al., 1996).

In view of the great importance to the thermal-hydraulic design of a thermal-control system in a space craft, a lot of pioneering researches have been performed for adiabatic and boiling two-phase flows under microgravity environment by means of a drop tower, an air craft, and a sounding-rocket to investigate the influence of the forces such as surface tension, momentum, and gravity or buoyancy on the two-phase flow dynamics (Keshock, 1987; Dukler et al., 1988; Colin et al., 1991; Lin and Rezkallah, 1995; Ohta et al., 1995; Straub and Micko, 1996). In a future, a thermal-hydraulic system analysis code under microgravity environment like that developed under normal gravity environment in the field of nuclear engineering should be developed for the detailed and precise thermal-hydraulic design and safety analysis of a thermal control system based on the two-fluid model. However, in order to close the two-fluid model, the interfacial transfer terms should be modeled accurately. In the present thermal-hydraulic system analysis codes developed under normal gravity environment, the effects of interfacial structure have been analyzed by using flow regimes and transition criteria. In this approach, no time or length scale is incorporated into the transition criteria. Such the approach causes a serious problem in calculating a developing flow. To solve such a problem, the introduction of the interfacial area transport equation has been recommended (Kocamustafaogullari and Ishii, 1995). The interfacial area transport equation can replace the traditional flow regime maps and regime transition criteria. The changes in the two-phase flow structure are predicted mechanistically by introducing the interfacial area transport equation. Thus, a successful development of the interfacial area transport equation can make a quantum improvement in the two-fluid model formulation.

From this point of view, continuous efforts have been made to develop the interfacial area transport equation (Hibiki and Ishii, 2000a,b; Hibiki et al., 2001) under normal gravity environment. In relation to the development of the interfacial area transport equation in bubbly flow under microgravity environment, this study aims at obtaining rigorous data sets on axial developments of flow parameters such as void fraction, bubble number density, interfacial area concentration, and Sauter mean diameter of adiabatic gas–liquid bubbly flows in a pipe under microgravity environment. These data are expected to be used for the development of reliable constitutive relations, which reflect the true transfer mechanisms in two-phase flow under microgravity environment.

2. Interfacial area transport equation in relatively small diameter pipe

The interfacial area transport equation can be deduced by considering the fluid particle number density transport equation analogous to Boltzmann's transport equation (Kocamustafaogullari and Ishii, 1995). By applying the cross-sectional area-averaging, the one-dimensional interfacial area transport equation becomes:

$$\frac{\partial a_i}{\partial t}+\frac{\mathrm{d}}{\mathrm{d}z}(a_i v_G)=\frac{1}{3\psi}\left(\frac{\varepsilon}{a_i}\right)^2(\phi_B-\phi_C+\phi_P)+\left(\frac{2a_i}{3\varepsilon}\right)\left\{\frac{\partial\varepsilon}{\partial t}+\frac{\mathrm{d}}{\mathrm{d}z}(\varepsilon v_G)\right\}=\Phi_B-\Phi_C+\Phi_P+\Phi_V,$$

$$\text{where}\quad \Phi_B\equiv\frac{1}{3\psi}\left(\frac{\varepsilon}{a_i}\right)^2\phi_B,\quad \Phi_C\equiv\frac{1}{3\psi}\left(\frac{\varepsilon}{a_i}\right)^2\phi_C,\quad \Phi_P\equiv\frac{1}{3\psi}\left(\frac{\varepsilon}{a_i}\right)^2\phi_P$$

$$\text{and}\quad \Phi_V\equiv\left(\frac{2a_i}{3\varepsilon}\right)\left\{\frac{\partial\varepsilon}{\partial t}+\frac{\mathrm{d}}{\mathrm{d}z}(\varepsilon v_G)\right\}. \tag{1}$$

The symbols of $a_i t$, $v_G z$, ψ, and ε denote the interfacial area concentration, the time, the interfacial velocity, the axial position, a factor depending on the bubble shape ($\psi = 1/(36\pi)$ for spherical bubbles), and the void fraction, respectively. ϕ_B, ϕ_C and ϕ_P are the rates of change of bubble number density due to bubble breakup, bubble coalescence, and phase change, respectively. Φ_B, Φ_C, Φ_P and Φ_V are the rates of change of interfacial area concentration due to bubble breakup, bubble coalescence, phase change, and void transport, respectively. Under no phase change condition, ϕ_P and Φ_P become zero. The sink and source terms of the interfacial area concentration, Φ_B and Φ_C should be modeled mechanistically based on possible bubble coalescence and breakup mechanisms.

In the previous study (Hibiki and Ishii, 2000a), the major mechanism of the interfacial area transport of adiabatic bubbly flow in medium pipes with inner diameters of 25.4 and 50.8 mm under normal gravity environment has been modeled successfully by the bubble coalescence due to the bubble random collisions driven by liquid turbulence and the bubble breakup due to the impact of turbulent eddies. However, the dominant mechanism of bubble coalescence in a small diameter pipe with an inner diameter of 9.0 mm was found to be wake entrainment from a visual observation (Hibiki et al., 2001). The difference in the bubble coalescence mechanism between medium and small pipes was attributed to relatively high bubble size-to-pipe diameter ratio, and restricted radial movement of bubbles in a small diameter pipe, which might not allow of bubble random collision. On the other hand, the visual observation suggested that for low liquid velocity the bubble breakup could be negligible because of weak turbulence (Hibiki et al., 2001). Thus, the mechanism of the interfacial area transport in a small diameter pipe for low liquid velocity under normal gravity environment could be modeled successfully by the bubble coalescence due to wake entrainment (Hibiki et al., 2001). Finally, the decrease rate of the interfacial area concentration, Φ_C is expressed as (Hibiki et al., 2001):

$$\Phi_C=\Gamma_C\left(\frac{8\Delta\rho g}{\rho_L}\right)^{1/3}\varepsilon^{1/3}(1-\varepsilon)^{1/3}a_i^{5/3}\left(\frac{j_G}{\varepsilon}-\frac{j_L}{1-\varepsilon}\right)^{2/3}\exp\left(\frac{K_C\rho_L^{1/2}D_b^{5/6}\varepsilon_T^{1/3}}{\sigma^{1/2}}\right), \tag{2}$$

where $\Delta\rho$, g, ρ_L, j_G, j_L, K_C, D_b, ε_T and σ are the density difference between phases, the gravitational acceleration, the liquid density, the superficial gas velocity, the superficial liquid velocity, a coefficient to be 1.29 for an air–water system, the bubble diameter, the energy dissipation rate per unit mass, and the surface tension, respectively. The adjustable valuable, Γ_C was determined to be 0.082 based on vertical adiabatic air–water bubbly flow data taken in the previous experiment using a 9 mm-diameter pipe (Hibiki et al., 2001) with the least squares method. The interfacial area transport equation with the sink term, Eq. (2), could predict interfacial area concentrations measured under the flow conditions of $0.013\ \mathrm{m/s} \leqslant j_G \leqslant 0.052\ \mathrm{m/s}$ and $0.58\ \mathrm{m/s} \leqslant j_L \leqslant 1.0\ \mathrm{m/s}$ within an average relative deviation of $\pm 11.1\%$ (Hibiki et al., 2001). It should be noted here that the decrease rate of the interfacial area concentration due to wake entrainment would be zero under microgravity environment because of $g \approx 0\ \mathrm{m/s^2}$ in Eq. (2).

3. Experiment

Two-phase flow experiments in this study were performed by using an underground-drop shaft at the Japan Micro-Gravity Center (JAMIC). Among many drop shafts in the world, the one at the JAMIC, which has the longest free-fall depth (490 m), would be the best facility in view of long duration of microgravity (about 10 s) and negligible residual gravity of 10^{-4}–10^{-5} G (1G = 9.8 $\mathrm{m/s^2}$, normal gravity). The characteristic performance of the JAMIC facility was detailed in our previous paper (Takamasa et al., 1996). Fig. 1 depicts the schematic diagram of a flow loop used in this experiment. The flow loop was installed in a drop capsule of the JAMIC facility. Working fluids were nitrogen gas and pure water, which was obtained by purifying tap water so as to an electrical conductivity lower than 1 μS/cm. Water started to be supplied into a 9 mm-inner diameter pipe using a gear pump at 20 s before the drop. Nitrogen gas started to be fed into the test channel from a gas tank at 7 s before the drop. The mixing chamber consisted of a double column made of acrylic tube and 7 mm-diameter Teflon tube bubble-generator with four holes of 0.6 mm diameter. Thus, bubbly flows under normal gravity (1G) and microgravity environments were generated for 7 s before the drop and 10 s during the drop, respectively. As the separation of gas from liquid was difficult during the microgravity experiment, the gas–liquid two-phase flow, which had passed through a test channel, was collected in a reservoir bag made of vinyl resin. The test loop was maintained at a system pressure of about 0.5 MPa to minimize the effect of the system pressure increase due to accumulated two-phase flow in the reservoir bag on the bubble volume. Pressure sensors, thermocouples, and flow sensors were used for measuring the pressure, the water temperature, and the water and nitrogen gas flow rates in the pipe, respectively. The superficial gas velocities, j_G at specific axial locations were calculated from gas flow rates, pressures and temperatures at the inlet and specific axial locations.

Viewing sections for taking bubble images were placed at four axial locations of $z/D = 7$, 30, 45, and 60. The outer surface of each viewing section was square, so as to prevent the distortion from the images. Axial changes of flow parameters such as void fraction, bubble number density, interfacial area concentration, and Sauter mean diameter were measured from the bubble images using the image-processing method. The methodology of the image-processing method was detailed in our previous paper (Takamasa et al., 1996). The measurement accuracy of interfacial area concentration was estimated to be within $\pm 6.95\%$ by a calibration experiment

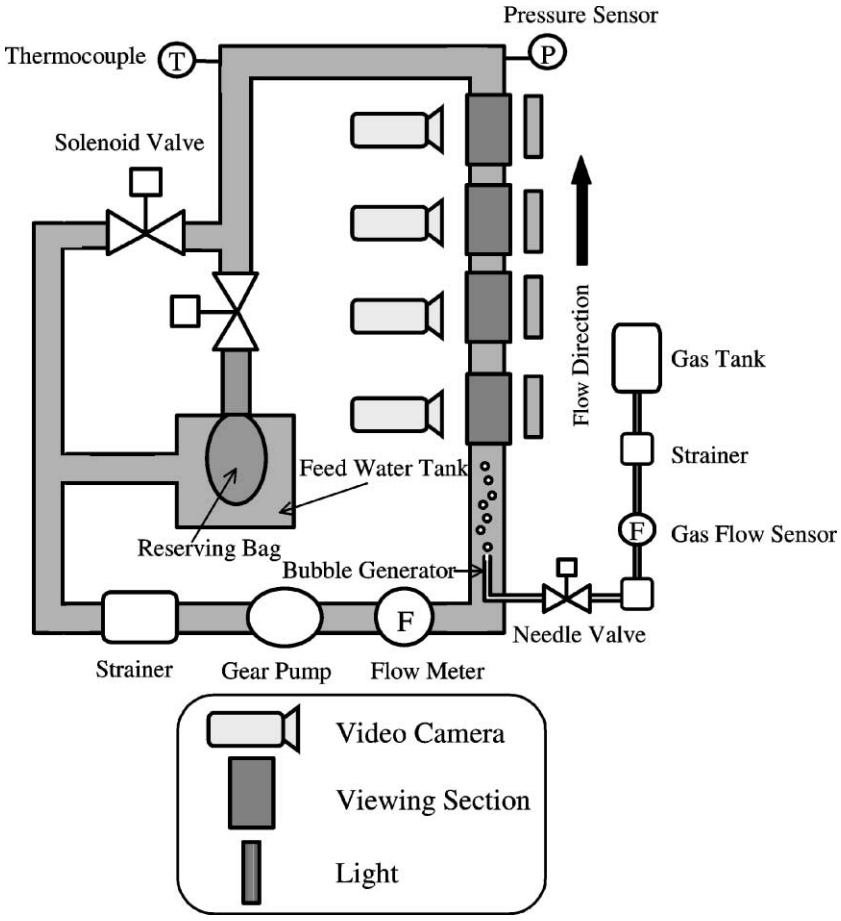

Fig. 1. Schematic diagram of flow loop.

Table 1
Experimental conditions

Superficial gas velocity, j_G (m/s)	Superficial liquid velocity, j_L (m/s)	Reynolds number, Re_L (–)	System pressure, P (MPa)
0.015	0.073	657	0.44
0.011	0.13	1170	0.45
0.018	0.12	1080	0.51
0.0083	0.20	1800	0.49
0.015	0.20	1800	0.51
0.022	0.22	1980	0.54

using a double sensor conductivity probe (Hibiki et al., 1998). A total of six data sets were acquired for flow conditions of 0.0083 m/s $\leqslant j_G \leqslant$ 0.022 m/s and 0.073 m/s $\leqslant j_L \leqslant$ 0.22 m/s (see Table 1).

4. Result and discussion

4.1. Effect of gravity on phase distribution

Before the discussion of one-dimensional axial interfacial area transport, bubble migration behavior under microgravity environment is discussed based on radial phase distribution data obtained by using a stereo-imaging method in the previous experiment (Takamasa et al., 1996). In the previous experiment, radial distributions of void fraction in turbulent air–water bubbly flows were measured under normal and micro gravity environments using the JAMIC facility (Takamasa et al., 1996). One interesting phenomenon in the vertical upward bubbly flow under normal gravity environment was that sliding bubbles existed near a channel wall under a certain flow condition. The purpose of the experiment was to clarify the migration mechanism of bubbles sliding near the wall. The specific role of the lift force, F_{Lift} pushing the bubbles towards the wall has not fully been understood yet. There are many theories to explain forces pushing the bubbles towards the wall. Some of them have explained that the lift force is generated by a bubble moving with a slip velocity as expressed by the following equation (Drew and Lahey, 1982):

$$F_{\mathrm{Lift}} = -C_{\mathrm{Lift}} v_{\mathrm{R}} \left(\frac{\partial v_{\mathrm{L}}}{\partial r} \right), \tag{3}$$

where $C_{\mathrm{Lift}}, v_{\mathrm{R}}$ and r are the lift coefficient, the slip velocity, and the radial position, respectively. When gravity varies from normal gravity to microgravity, the interaction between the two phases should change in the sliding bubbly flow due to reduced slip velocity between two phases. If Eq. (3) holds for any bubbles, lateral migration of any bubbles should disappear. Since Eq. (3) is proportional to the relative velocity, bubbles should rise almost rectilinearly as the relative velocity decreases. The experimental result under normal and microgravity environments showed that there were some sliding bubbles whose tails attached to the wall sublayer under normal gravity environment and no such bubbles under microgravity environment. Bubbles under mi-

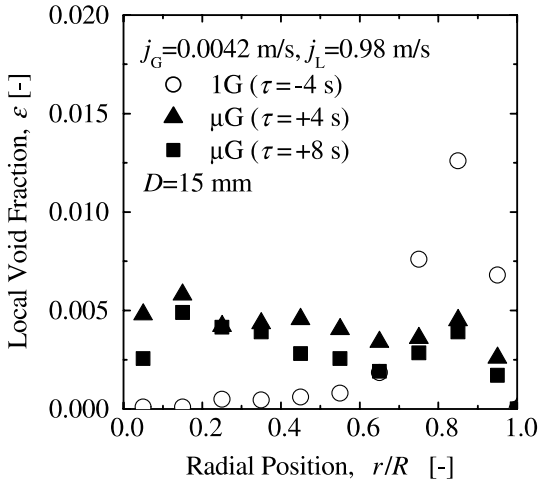

Fig. 2. Void-fraction distribution under normal and microgravity environments.

crogravity environment were almost spherical, which meant that negligible vertical and lateral stresses worked on the bubbles. An example of the effect of gravity on radial void-fraction distribution is shown in Fig. 2. In the figure, τ is the passage time after the drop, and open circles, solid triangles, and solid squires indicate the void fractions measured under normal gravity environment at 4 s before the drop, and under microgravity environment at 4 and 8 s after the drop started, respectively. As shown in the figure, a wall peaking in the void-fraction distribution observed under normal gravity environment disappeared under microgravity environment. Under normal gravity environment reestablished after the end of the drop, the sliding bubbles and the wall peaking in the void-fraction distribution were observed again. This result may support the lift force model as represented by Eq. (3).

4.2. Visual observation of flow development

Fig. 3 shows images of axial development of a bubbly flow ($j_G = 0.015$ m/s and $j_L = 0.20$ m/s) under microgravity environment. The bubble coalescence caused the increase in the bubble size and the decrease in the bubble number density. Fig. 4 shows sequential images taken at $z/D = 7$, which capture typical bubble coalescence under microgravity environment. The flow condition in Fig. 4 is $j_G = 0.015$ m/s and $j_L = 0.073$ m/s. The figure reveals that bubble coalescence occurs even under low liquid flow rate and microgravity conditions where the bubble random collision and wake entrainment models suggest negligible bubble coalescence. This figure clearly shows the bubble coalescence mechanism such that the trailing bubble captures the proceeding bubble. Such bubble collision mechanism (velocity-profile entrainment) is apparently similar to wake entrainment which may not be observed under microgravity environment. Therefore, a peculiar mechanism to cause the bubble coalescence may exist under microgravity environment.

In the previous experiment using a 9 mm-diameter pipe under normal gravity environment, flat radial distributions in the gas velocity were found due to bubble-induced turbulence and relatively high bubble diameter-to-pipe diameter ratio (Hibiki et al., 2001). On the other hand, in the present experiment under microgravity environment, negligible local slip velocity between the phases might generate negligible bubble-induced turbulence resulting in radial gas-velocity distribution similar to respective liquid velocity distribution. In the tested flow condition under microgravity environment, the liquid velocities are very low ($651 \leqslant Re_L \leqslant 1980$) and bubble-induced turbulence may be negligible, so that the liquid-velocity distribution is probably similar to that in a laminar single-phase flow, where the liquid velocity near the pipe center is much faster than that near the wall. Thus, marked velocity difference possibly exists between bubbles near the pipe center and those near the wall. Sweeping faster trailing bubbles near the pipe center out slower preceding bubbles near the wall is likely to cause a pseudo-wake entrainment effect, namely a velocity-profile entrainment effect in low liquid velocity under microgravity environment. However, the decrease in the bubble diameter-to-pipe diameter ratio possibly deteriorates the velocity-profile entrainment, since the projected area of the trailing bubble may not sweep that of the preceding bubble out for low bubble diameter-to-pipe diameter ratio. The increase in the liquid velocity is also expected to decrease this velocity-profile entrainment effect, since the liquid-velocity distribution in a turbulent flow may not produce significant velocity difference between bubbles near the channel center and wall. Fig. 5 shows the dependence of the bubble coalescence due to velocity-profile entrainment on Reynolds number of the liquid phase, Re_L. When no bubble coalescence

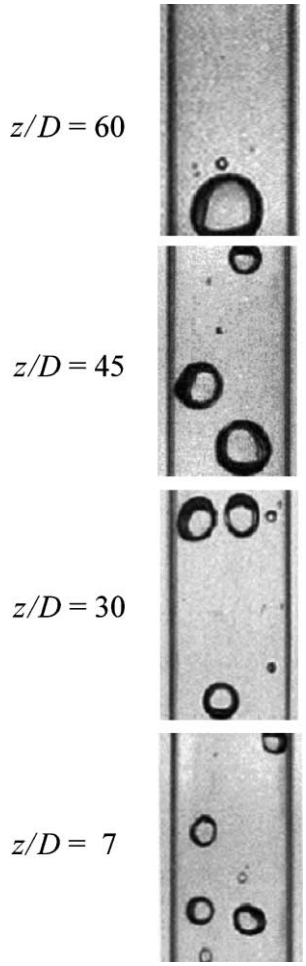

Fig. 3. Axial development of bubbly flow under microgravity environment ($j_G = 0.015$ m/s, $j_L = 0.20$ m/s).

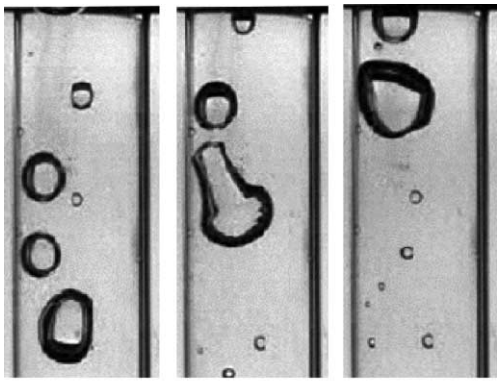

Fig. 4. Bubble coalescence under microgravity environment ($j_G = 0.015$ m/s, $j_L = 0.073$ m/s, $z/D = 7$).

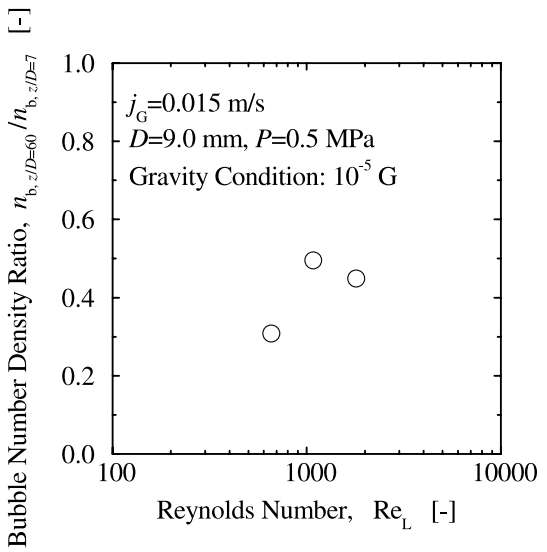

Fig. 5. Dependence of bubble coalescence due to velocity-profile entrainment on Reynolds number of liquid phase.

occurs between two measuring stations at $z/D = 7$ and 60, the ratio of bubble number density at $z/D = 60$ to that at $z/D = 7$ takes a value at 1. As can be seen from this figure, the ratio of bubble number density at $z/D = 60$ to that at $z/D = 7$ tends to increase with Reynolds number, which means that the increase in Reynolds number, namely the deterioration in the steepness of the liquid-velocity distribution hinders the bubble coalescence. This result implicitly supports the velocity-profile entrainment mechanism. However, it should be noted here that for very high Reynolds number, large energy-containing eddy might possibly enhance the axial bubble motion, resulting in bubble coalescence. In a future, further study should be addressed on the bubble coalescence mechanism for high Reynolds number.

4.3. Axial development of flow parameters

Figs. 6–9 show axial changes of one-dimensional void fraction, bubble number density, interfacial area concentration, and Sauter mean diameter measured under microgravity environment, respectively. Lines in Fig. 8 indicate the interfacial area concentrations predicted by the interfacial area transport equation, Eqs. (1) and (2) with the assumption of a normal gravity condition for respective flow condition. Thus, the lines represent the interfacial area transports to be observed under respective flow and normal gravity conditions, and the difference between the lines and interfacial area concentrations measured under microgravity environment shows the effect of gravity on the interfacial area transport. As shown in Fig. 6, the void fraction does not change along the axial direction, because of negligible friction loss and no static head change. On the other hand, as the flow develops, marked bubble coalescence decreases the bubble number density significantly (see Fig. 7). This leads to the decrease in the interfacial area concentration and the increase in the Sauter mean diameter (see Figs. 8 and 9).

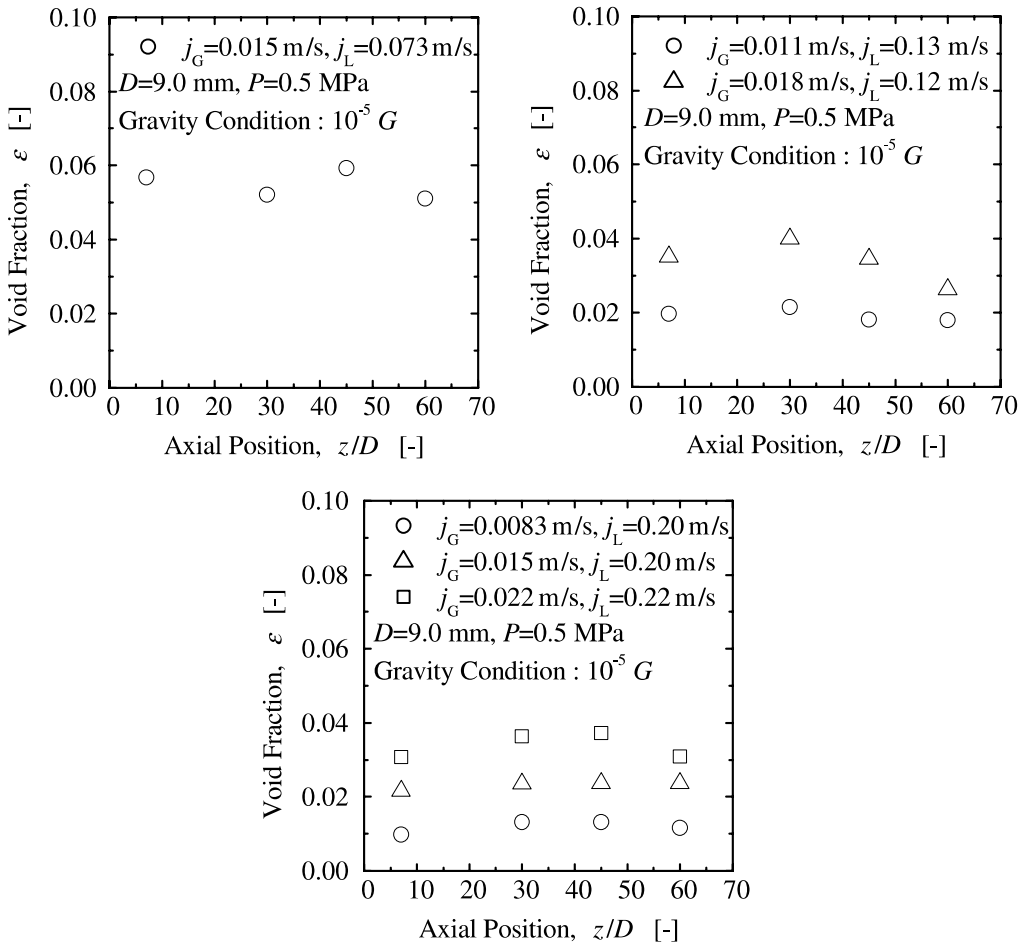

Fig. 6. Axial development of void fraction.

Typical changes of the interfacial area concentrations along the flow direction due to each mechanism are shown in Fig. 10. In the figure, open circles are measured interfacial area concentrations, and solid, broken and dotted lines indicate the total interfacial area concentration change to be expected under normal gravity environment, the interfacial area concentration change due to pressure change, and the interfacial area concentration change due to wake entrainment to be observed under normal gravity environment, respectively. The decrease rate of the interfacial area concentration due to wake entrainment indicated by dotted lines is calculated by Eq. (2) with the assumption of a normal gravity condition. If bubble coalescence and breakup do not occur, the axial change in the interfacial area concentration should be represented by the broken lines. The difference between measured interfacial area concentrations and predicted ones indicated by the broken lines shows the effect of gravity on the interfacial area transport. Incidentally, the velocity-profile entrainment effect under microgravity environment is comparable to the wake entrainment effect under normal gravity environment in the tested flow conditions. This

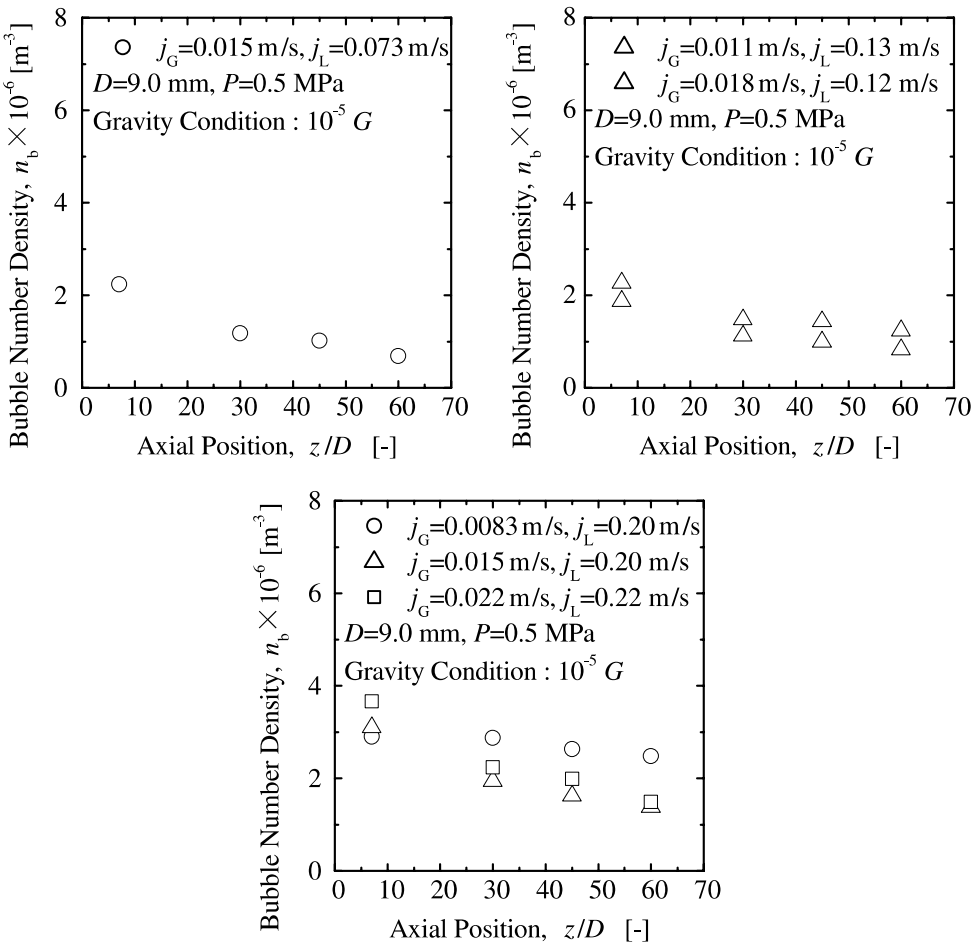

Fig. 7. Axial development of bubble number density.

leads to insignificant difference between measured interfacial area concentrations and ones predicted by the interfacial area transport equation with the wake entrainment model under normal gravity environment apparently. However, possible bubble coalescence mechanism would be different between normal gravity and microgravity conditions. In a future study, a velocity-profile entrainment model should be developed by taking into account the velocity difference between bubbles near the channel center and wall.

5. Conclusions

Axial developments of one-dimensional void fraction, bubble number density, interfacial area concentration, and Sauter mean diameter of adiabatic nitrogen–water bubbly flows in a 9 mm-diameter pipe were measured by using an image-processing method under microgravity

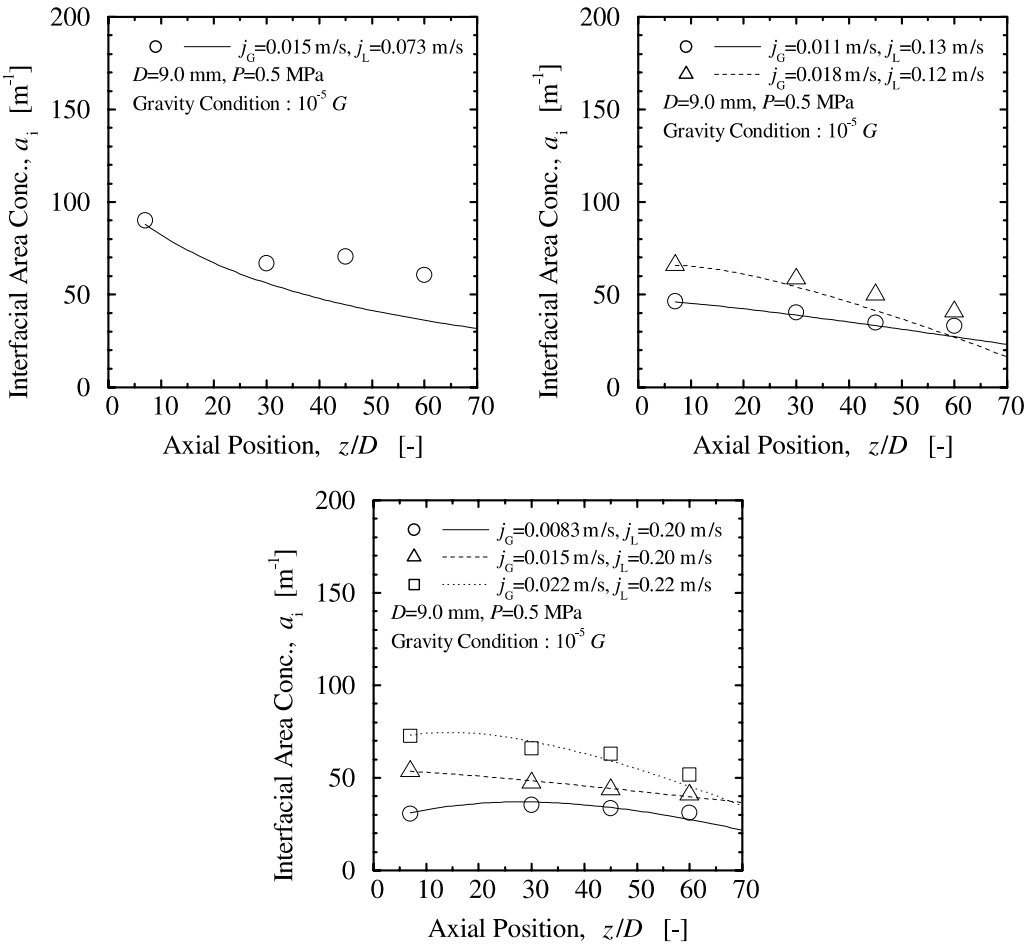

Fig. 8. Axial development of interfacial area concentration.

environment. The flow measurements were performed at four axial locations (axial distance from the inlet normalized by the pipe diameter = 7, 30, 45 and 60) under various flow conditions of superficial gas velocity (0.0083–0.022 m/s) and superficial liquid velocity (0.073–0.22 m/s). The interfacial area transport mechanism was discussed by the visual observation. Marked bubble coalescence occurred due to sweeping trailing bubbles near the channel center out preceding bubbles in the vicinity of the channel wall (velocity-profile entrainment). Negligible bubble breakup was observed because of weak turbulence under tested flow conditions. Axial changes of measured interfacial area concentrations were compared with the interfacial area transport equation considering the bubble expansion and the wake entrainment to be observed under normal gravity environment. Incidentally, the velocity-profile entrainment effect under micro-gravity environment was likely to be comparable to the wake entrainment effect under normal gravity environment in the tested flow conditions. This led to insignificant difference between measured interfacial area concentrations and ones predicted by the interfacial area transport equation with the wake entrainment model under normal gravity environment, apparently.

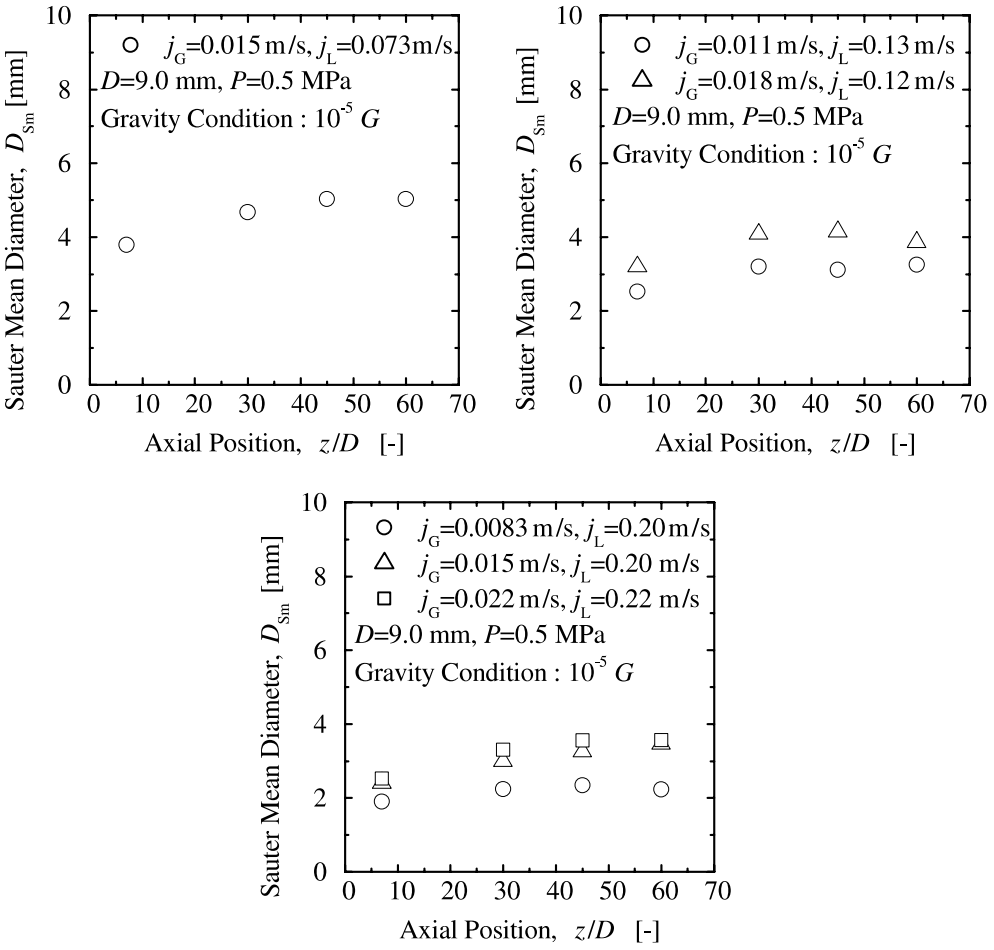

Fig. 9. Axial development of Sauter mean diameter.

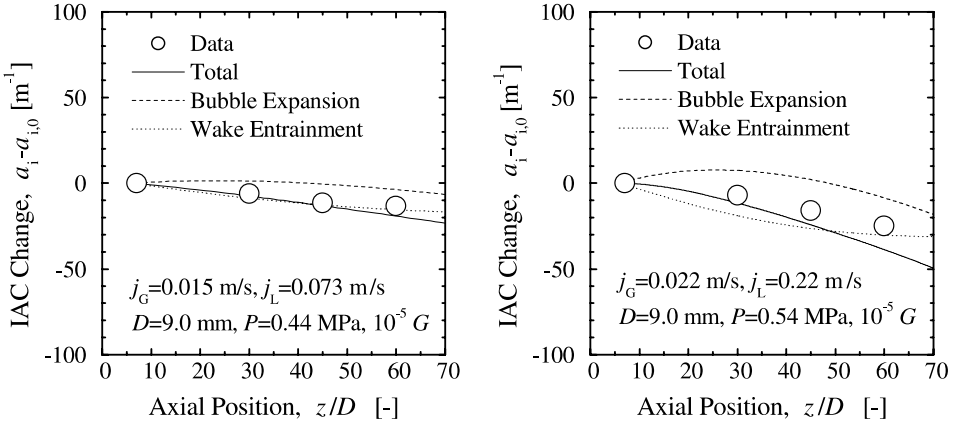

Fig. 10. Contributions of bubble expansion and wake entrainment to interfacial area transport.

However, possible bubble coalescence mechanism would be different between normal gravity and microgravity conditions.

Acknowledgements

The authors wish to thank Japan Space Utilization Promotion Center (JSUP) and New Energy Development Organization (NEDO) in Japan for their financial supports on this project. Part of this work was supported by the Ministry of Education, Science, Sport and Culture (no. 14580542).

References

Colin, C., Fabre, J., Dukler, A.E., 1991. Gas–liquid flow at microgravity conditions—1. Int. J. Multiphase Flow 17, 544–553.

Di Marco, 1997. Overview and prospects of boiling heat transfer studies in microgravity. In: Proceedings of INSPACE '97, Tokyo, Japan, pp. 1–14.

Drew, D.A., Lahey Jr., R.T., 1982. The vertical mass and lift force on a sphere in rotating and straining flow. Int. J. Multiphase Flow 7, 113–121.

Dukler, A.E., Fabre, J.B., Mcquillen, J.B., Vernon, R., 1988. Gas–liquid flow at microgravity condition: flow patterns and their transitions. Int. J. Multiphase Flow 14, 389–400.

Grigoriev, Y.I., Grogorov, E.I., Cykhotsky, V.M., Prokhorov, Y.M., Gorbenco, G.A., Blinkov, V.N., Teniakov, I.E., Malukihin, C.A., 1996. Two-phase heat transport loop of central thermal control system for the international space station "Alpha" Russian segment. In: AIChE Symposium Series—Heat Transfer. vol. 310, pp. 9–17.

Hibiki, T., Ishii, M., 2000a. One-group interfacial area transport of bubbly flows in vertical round tubes. Int. J. Heat and Mass Transfer 43, 2711–2726.

Hibiki, T., Ishii, M., 2000b. Two-group interfacial area transport equations at bubbly-to-slug flow transition. Nuclear Engineering Design 202, 39–76.

Hibiki, T., Hogsett, S., Ishii, M., 1998. Local measurement of interfacial area, interfacial velocity and liquid turbulence in two-phase flow. Nuclear Engineering Design 184, 287–304.

Hibiki, T., Takamasa, T., Ishii, M., 2001. Interfacial area transport of bubbly flow in a small diameter pipe. Journal of Nuclear Science and Technology 38, 614–620.

Keshock, E.G., 1987. Two-phase flow tests conducted under normal and zero-gravity (KC-135 Aircraft) conditions. Final Report, NASA Contract NAS9-17195.

Kocamustafaogullari, G., Ishii, M., 1995. Foundation of the interfacial area transport equation and its closure relations. Int. J. Heat and Mass Transfer 38, 481–493.

Lin, Y.M., Rezkallah, K.S., 1995. Numerical predictions of turbulence structure in gas–liquid bubbly flows under normal and microgravity conditions. In: Proceedings of 2nd International Conference on Multiphase Flow. vol. 6, pp. 21–26.

Ohta, H., Inoue, K., Yamada, Y., Yoshida, S., Fujiyama, H., Ishikura S., 1995. Microgravity flow boiling in a transparent tube. In: Proceedings of ASME/JSME Thermal Engineering Conference. vol. 4, pp. 547–554.

Straub, J., Micko, S., 1996. Boiling on a wire under microgravity conditions: First Results from a Space Experiment Performed in 1996. In: Gorenflo, D., Kenning, D.B.R., Marvillet, C., Paderborn, D. (Eds.), Proceedings of EUROTHERM Seminar. vol. 48, Pool Boiling 2, pp. 275–282.

Takamasa, T., Watarai, M., Kondo, K., 1996. Gas water bubbly flow under microgravity condition. In: Proceedings of 31st ASME/ANS/AIAA National Heat Transfer Conference. In: AIChE Symposium Series 310/92, pp. 180–185.